Molecular Systems Biology 4; Article number 234; doi:10.1038/msb.2008.70
Citation: *Molecular Systems Biology* 4:234

www.molecularsystemsbiology.com

molecular systems biology

Robust and sensitive control of a quorum-sensing circuit by two interlocked feedback loops

Joshua W Williams[1], Xiaohui Cui[1], Andre Levchenko[2,*] and Ann M Stevens[1,*]

[1] Department of Biological Sciences, Virginia Tech, Blacksburg, VA, USA and [2] Department of Biomedical Engineering, Johns Hopkins University, Baltimore, MD, USA
* Corresponding authors. A Levchenko, Department of Biomedical Engineering, Johns Hopkins University, 208C Clark Hall, 3400 N Charles Street, Baltimore, MD 21218, USA. Tel.: +1 410 516 5584; Fax: +1 410 516 4771; E-mail: alev@jhu.edu or AM Stevens, Department of Biological Sciences, Virginia Tech, 219 Life Sciences 1 (0910), Washington Street, Blacksburg, VA 24061, USA. Tel.: +1 540 231 9378; Fax: +1 540 231 4043; E-mail: ams@vt.edu

Received 12.3.08; accepted 24.10.08

The quorum-sensing (QS) response of *Vibrio fischeri* involves a rapid switch between low and high induction states of the *lux* operon over a narrow concentration range of the autoinducer (AI) 3-oxo-hexanoyl-L-homoserine lactone. In this system, LuxR is an AI-dependent positive regulator of the *lux* operon, which encodes the AI synthase. This creates a positive feedback loop common in many bacterial species that exhibit QS-controlled gene expression. Applying a combination of modeling and experimental analyses, we provide evidence for a LuxR autoregulatory feedback loop that allows LuxR to increase its concentration in the cell during the switch to full *lux* activation. Using synthetic *lux* gene fragments, with or without the AI synthase gene, we show that the buildup of LuxR provides more sensitivity to increasing AI, and promotes the induction process. Elevated LuxR levels buffer against spurious variations in AI levels ensuring a robust response that endows the system with enhanced hysteresis. LuxR autoregulation also allows for two distinct responses within the same cell population.
Molecular Systems Biology 16 December 2008; doi:10.1038/msb.2008.70
Subject Categories: simulation and data analysis; signal transduction
Keywords: bistability; hysteresis; *lux* operon; quorum sensing; *Vibrio fischeri*

Introduction

Quorum sensing (QS) is an example of cell–cell communication in bacteria, allowing an assemblage of closely positioned cells to alter its behavior in a coordinated manner, if the cell density exceeds a specific threshold. QS regulates a plethora of critically important phenotypes, including antibiotic production, release of exoenzymes, production of virulence factors, induction of genetic competency, conjugative plasmid transfer, biofilm formation and bioluminescence (Fuqua *et al*, 2001; Waters and Bassler, 2005; Reading and Sperandio, 2006). In addition to understanding the role of these bacterial phenotypes to pathogenic and symbiotic states, analysis of the mechanisms underlying QS might shed light on how the behavior of a single cell can be tightly and robustly coordinated with the behavior of the cell group.

The QS response of *Vibrio fischeri* is a model system for many other QS systems that share networks similar to the LuxR/I network (Taga and Bassler, 2003). LuxR is an autoinducer (AI)-dependent positive regulator of the *lux* operon, and LuxI produces the AI molecule, 3-oxo-hexanoyl-L–homoserine lactone. Much is known about how the LuxR/I system achieves activation of the *lux* operon leading to bioluminescence. A number of factors, including the activator complex cAMP–CRP, regulate the expression of *luxR* (Friedrich and Greenberg, 1983; Dunlap and Greenberg, 1985, 1988). LuxR then activates expression of the *lux* operon when the concentration of LuxR–AI complexes reaches a critical threshold. This leads to higher levels of AI, generating a positive feedback loop (Dunlap and Greenberg, 1988; Choi and Greenberg, 1992; Stevens and Greenberg, 1999; Lupp *et al*, 2003). It has been proposed that LuxR not only regulates the *lux* operon but it might also positively or negatively autoregulate the QS response through modulating its own expression (Dunlap and Ray, 1989; Shadel and Baldwin, 1991, 1992; Chatterjee *et al*, 1996), although the precise molecular basis for this autoregulation remains unknown.

The presence of one or more feedback interactions in the molecular networks underlying QS in *V. fischeri* and other bacterial systems might lead to such emergent properties as hysteretic responses and the associated 'memory' of the previous network states. Such memory-like properties have been suggested for other systems containing positive feedback interactions, based both on mathematical modeling and experimental investigation (Ferrell, 2002; Levchenko, 2003; Sha *et al*, 2003; ; Angeli *et al*, 2004; Ninfa and Mayo, 2004;

Ozbudak *et al*, 2004). Some mathematical models of *V. fischeri* QS signaling have suggested the existence of hysteresis in response to extracellular AI concentration ([AI]), based on AI-induced *luxI* expression leading to a further increase in AI production (James *et al*, 2000; Cox *et al*, 2003; Goryachev *et al*, 2006; Muller *et al*, 2006). This positive feedback is reliant on retention and accumulation of AI in the cell milieu. However, as the AI can freely diffuse across the cell membrane (Kaplan and Greenberg, 1985) this can make the system vulnerable to potentially rapid changes in [AI]. In a classical hysteresis analysis, the [AI] is exogenously fixed at various levels. This can mask the feedback-based increase of [AI], and hence complicate the experimental and theoretical analysis of the effects of the positive LuxI-based feedback.

Because the mechanism of LuxR autoregulation in *V. fischeri* is unknown, the analysis of the onset of QS has been based on various assumptions (Shadel and Baldwin, 1991, 1992; Minogue *et al*, 2002). If this autoregulation is indeed present, its role in the QS response is presently not clear. In this report, through a combination of modeling and experiments, we provide further evidence for the existence of this second feedback circuit in the *luxR/I* QS network. Moreover, we demonstrate the presence of hysteresis in a reduced *lux* network lacking LuxI-based feedback. In the network containing both feedback interactions, *luxR*-positive autoregulation can enhance response diversification and endow it with higher robustness to AI perturbation, thereby increasing the fidelity of the QS switch.

Results

Decoupling LuxI-mediated positive feedback

A convenient way to computationally and experimentally analyze feedback loops is to decouple them. For the example of *lux* operon regulation, the [AI] can be held at a fixed value, and the resulting expression of the system can be determined. This analysis can be repeated for different [AI] values, yielding curves showing dependencies of *luxI* expression on AI ([LuxI]=f([AI])) or AI production on LuxI ([AI]=g([LuxI])). These curves, known as null clines of the underlying dynamical system, can intersect when plotted in the same coordinate system (e.g. by co-plotting f and g^{-1}), revealing points corresponding to the steady-state concentrations of AI and LuxI in the reconstituted feedback system (Figure 1A). Depending on how nonlinear the functions f and g^{-1} are, they can intersect in various ways, yielding a different number of steady states, which can be either stable, (i.e. resistant to small concentration changes due to molecular noise or other random perturbations) or unstable (Angeli *et al*, 2004). Multiple steady states signal that the response can stably display different values, depending on the initial conditions of the systems (e.g. whether the initial [AI] is high or low). In the presence of many AI-secreting cells, the [AI] experienced by individual cells would be the sum of endogenously produced LuxI-mediated AI (AI_{in}) and AI diffusing from other cells (AI_{ex}). Additionally, AI_{ex} can be controlled experimentally, by supplying synthetic AI. The presence of AI_{ex} can further lead to a shift of the g null cline by uniform addition of AI_{ex}: $g'=g+[AI_{ex}]$. This shift can lead to a change in the number of the steady states, allowing for a fast transition from low to high values of the response. For the complete *lux* operon, this would imply the frequently assumed hysteretic (history dependent)

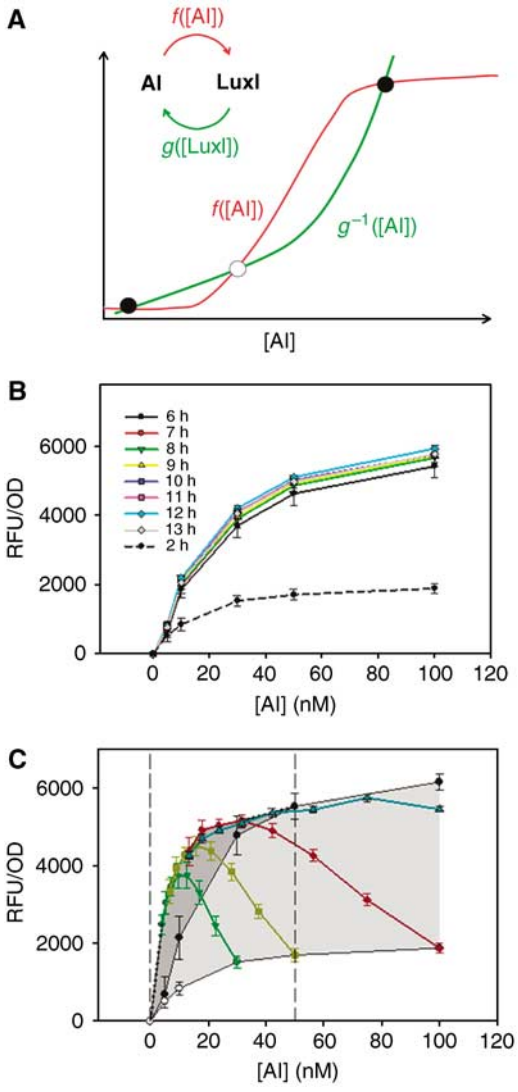

Figure 1 Analysis of GFP expression in the *lux01* circuit in response to different AI concentrations. (**A**) An illustrative cartoon of a decoupled LuxI–AI-positive feedback system. One can find possible stable steady-state responses in a positive feedback circuit by separately analyzing how AI regulates LuxI and how LuxI regulates AI. The resulting dependencies, or null clines: f([AI]) and g([*LuxI*]), can be plotted together, with the intersection points yielding the steady states, which can be stable (closed circles) or not (open circle). (**B**) Analysis of the f([AI]) null cline by allowing the response of the *lux01* circuit to reach steady states after the addition of different exogenously added [AI], for different amounts of time. The data are expressed as relative fluorescence units/optical density of the culture. Error bars represent the standard deviation between two independent triplicate data sets. (**C**) Analysis of the f([AI]) null cline by allowing the response of the *lux01* circuit to reach steady state after dilution from high initial induction values (reached at 8 h after instantaneous 25% serial dilution from 6 h incubation in 100 nM [AI]) (blue triangles). This response is overlaid with the results of the 6 h incubation obtained in (B) (closed circles) and the area between the curves is shaded dark gray. The area between the 2 and 6 h induction curves in (C) is shaded light gray. The results of the 25% hourly dilution experiments from cultures initially induced for 2 h at different exogenous [AI] (30 nM, inverted triangles; 50 nM, squares; 100 nM, rhombi) prior to dilution are also shown. Error bars represent the standard deviation between two independent triplicate data sets.

behavior, and a rapid onset of QS beyond a critical cell density.

Previous analyses suggested that at least one of the null clines f or g^{-1} should be sufficiently nonlinear for multiple steady states to occur (Ferrell, 2002; Tyson *et al*, 2003; Angeli *et al*, 2004). To determine the properties of the f null cline, an *Escherichia coli* strain was created with a chromosomal insertion of a synthetic *lux01* genetic circuit capable of expressing LuxR, but with a truncated divergently transcribed *lux* operon, so that all of the transcripts normally downstream of the promoter are replaced with *gfp*. Thus exogenous AI is required for GFP expression (Supplementary Figure S1). This allowed decoupling of the AI-LuxI feedback and experimental measurement of the f null cline under different conditions. Using the *lux*01 circuit, the steady-state GFP expression values for various [AI] were determined by increasing AI from 0 up to 100 nM (Figure 1B). The resulting nonlinear steady-state response curves provided an estimate of the true f null cline (henceforth referred to as f_L). This experiment also established that the *lux*01 circuit became maximally induced after about 6 h under the conditions used. When AI was diluted from the media of the cells in a highly induced state (7 h incubation at 100 nM AI), either instantaneously to lower [AI] or through hourly 25% dilutions, the resulting, virtually identical response curves were distinct from f_L in the 0–50 nM AI range when compared with cultures that were induced but not diluted (this higher response curve, referred to as f_H, was identical with f_L in the 50–100 nM AI range; Figure 1C). Furthermore, when AI_{ex} was gradually diluted at an hourly rate of 25% from cells stimulated to less than the maximally induced state (2 h incubation at 30, 50 or 100 nM), cellular GFP concentration transiently increased over time in all three cases, converging to and closely following the upper response curve f_H (Figure 1C). This suggests that the cells remained in the higher state of induction while undergoing continual loss of AI_{ex}, until a critical threshold was met, at which point the cells began to return to the lower induction state. In combination, these results suggested that the response could stably converge to different response curves, f_L and f_H, following different types of *lux01*circuit induction, and thus that the particular shape of the f null cline was dependent on the initial induction state of the cells.

LuxR-mediated positive feedback is supported by experimentation and modeling

It has been proposed earlier that LuxR can transcriptionally regulate its own expression (Dunlap and Ray, 1989; Shadel and Baldwin, 1991, 1992; Chatterjee *et al*, 1996). To determine the dependence of *luxR* transcription on $[AI_{ex}]$, qRT–PCR analysis was performed on RNA samples extracted from cells with steady-state GFP expression corresponding to the lower branch of the hysteresis graph (i.e. induced from 0 to maximum with 100 nM AI; Figure 1C). In the range of 0–30 nM AI, *luxR* transcription varied as a function of exogenous AI, and there was an increase in *luxR* mRNA that reached a maximum level at exogenous [AI] above 10 nM (Figure 2). These findings are consistent with the proposed AI-dependent LuxR-controlled hysteretic autoregulation of *luxR* and support the hypothesis that the second feedback loop suggested by the data could be due to positive LuxR transcriptional autoregulation.

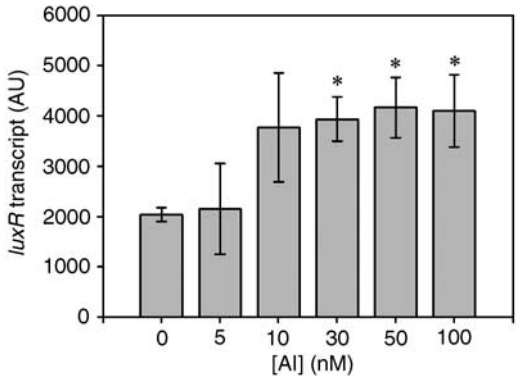

Figure 2 Validation of induced *luxR* expression by qRT–PCR analysis of *luxR* transcript levels in the *lux01* circuit. qRT–PCR analysis of *luxR* transcript quantity was performed on undiluted MG1655-01S induced for 6 h at [AI] of 5, 10, 30, 50 and 100 nM. Error bars represent the standard deviation between three independent triplicate data sets. Asterisks indicate data values that are significantly higher than that of the 5 nM data with a $P<0.025$ (standard *t*-test).

To further bolster this hypothesis and explore the underlying putative regulatory mechanism, a simple mathematical model of LuxR autoregulation in the *lux01* circuit was developed. This model investigated two distinct possibilities: the presence and absence of LuxR-positive autoregulation encoded in this simplified *lux* network using two corresponding systems of ordinary differential equations. In both cases, plus or minus LuxR-positive autoregulation, the corresponding models could be treated analytically, allowing us to derive a number of conclusions without explicit definition of the model parameter values, many of which are still unknown. The model postulating a positive feedback was based on the following assumptions, for which there is some experimental basis: (1) expression of LuxR is regulated by both LuxR–AI complexes and cAMP–CRP; (2) the stoichiometry of the LuxR · AI complex is such that two molecules of LuxR are coupled to two molecules of AI; (3) there is a non-zero, basal, AI-independent synthesis of LuxR. In the model analysis, we have examined the influence of these assumptions on the properties of the output using the following system of differential equations:

$$\begin{cases} \frac{dR}{dt} = c_0 + \frac{k_1 C}{C+K_D} - k_2 R - k_5 R \cdot A + k_6(\mathrm{RA}), \\ \frac{dC}{dt} = k_3(\mathrm{RA})^2 - \mathrm{k_4 C}, \\ \frac{d(RA)}{dt} = k_5 R \cdot A - k_6(\mathrm{RA}) - 2\mathrm{k_3}(\mathrm{RA})^2 + 2\mathrm{k_4 C} \end{cases} \quad (1)$$

In this system, the first equation describes the rate of change of the concentration of LuxR (denoted as R), which positively depends on the sum of the basal (c_0) and auto-induced synthesis rates and negatively depends on constitutive degradation and dilution due to cell division. The inducible synthesis rate, described by the second term of the first equation, is assumed to be proportional to the probability of transcriptional initiation controlled by the $(\mathrm{LuxR} \cdot \mathrm{AI})_2$ complex (C) binding to the corresponding binding site in the regulatory sequence of the operon with the dissociation constant K_D. The second and third equations describe the formation of the LuxR · AI complex through formation of the intermediate bi-molecular LuxR · AI complex (RA), which can

either dissociate or form a more stable ternary molecular complex *C*. The [AI] is denoted as *A*. In the model (1), we assume constant glucose concentration, leading to no regulatory role of cAMP–CRP. CRP-mediated regulation is explored in an expanded model below. For this analysis, it is important that LuxR dimerizes to form the complex C, whereas the exact stoichiometry of the complex with respect to the number of AI molecules is not consequential. The same results would be valid if *C* was tri-molecular, with one molecule of AI and two molecules of LuxR.

At steady state, all derivatives in the systems (1) are equal to zero, which converts both systems into the same system of algebraic equations, which in turn can be reduced, with $\gamma=k_1/k_2$, $\delta=c_0/k_2$ and $\beta=K_D/\alpha A^2$, to the following form:

$$-R^3+(\delta+\gamma)R^2-\beta R+\delta\beta=0 \qquad (2)$$

The steady-state levels of *luxR* expression are obtained by solution of equation (2), which has three roots. One can further show that two of the steady states are stable and one is unstable, further implying that the system is indeed bistable.

To determine the bifurcation diagram defined by (2), the method used by Ozbudak *et al* (2004) was applied. At the boundary between the monostable and bistable regimens, two of the three solutions to (2) coincide. Denoting them as a and denoting the third, distinct, solution as θa, one has $(y-a)(y-a)(y-\theta a)$, or

$$y^3-(2+\theta)a\,y^2+(1+2\theta)\,a^2\,y-\theta\,a^3=0 \qquad (3)$$

Comparing the coefficients in this equation with those in (2), one can obtain the following system of parametric equations for the parameters γ, δ and β:

$$\begin{cases}\frac{\delta+\gamma)^2}{\beta}=\frac{(2+\theta)^2}{1+2\theta}\\ \frac{\gamma}{\delta}=\frac{2(1+\theta)^2}{\theta}\end{cases} \qquad (4)$$

Both parameters, $(\gamma+\delta)^2/\beta$ and $\mu=\gamma/\delta$ are non-dimensional. Using (4) one can create the bifurcation diagram in Figure 3A. It is apparent from this diagram that, for certain combinations of parameters, two steady states can coexist for the expression levels of *luxR*, and by extension, those of GFP expression in the *lux01* strain. Raising the concentration of the exogenous [AI] is equivalent to 'moving' on this diagram parallel to the *X* axis from the far left uninduced state to the far right induced state with a transition through a bistable regimen (dashed line with arrows). Importantly, for this type of transition, the ratio $\mu=\gamma/\delta=k_1/c_0$ (i.e. the ratio of the strengths of inducible and constitutive transcription) has to be greater than approximately 8.

The strength of inducible transcription is regulated, in part, by the occupancy of the CRP-binding site, and thus by the level of glucose, as absence of glucose activates CRP. As the concentration of glucose increases, the occupancy of the CRP site decreases, and the bistability regimen may exist in a progressively narrower range of $[AI_{ex}]$. To account for this, the system (1) must be modified to explicitly include the effect of cAMP–CRP binding. Following the example of Buchler *et al* (2003), we can write for the equivalent of equation (3):

$$c_0+\frac{k_1\alpha R^2A^2k_7P}{\alpha R^2A^2+K_D+k_7PK_D+k_7P\alpha R^2A^2}-k_2R=0 \qquad (5)$$

Here, P denotes the concentration of active CRP and k_7 is the equilibrium association constant of cAMP–CRP binding to its cognate-binding site. Making the substitution: $\eta=k_7P$, present in equation (5), leads to:

$$R^3-(\gamma w+\delta)R^2+\beta R-\delta\beta=0 \qquad (6)$$

where the weight $w=\eta/(1+\eta)$ varies between zero and unity, as CRP varies from zero to maximal values. Variation of the contribution of γ to equation (5) is equivalent to raising or lowering along the Y axis the 'trajectory' describing the response to AI variation in the bifurcation diagram above, with the trajectory itself being parallel to the X axis. In particular, increasing the glucose levels would be equivalent to moving the trajectory lower. Ultimately, when $w\gamma/\delta$ levels become less than approximately 8, bistability is lost.

In an alternative model, no positive autoregulation of *luxR* expression is assumed. This corresponds to equating k_1 to zero in (1), thus the value of $\gamma=0$. As seen above, this implies no bistability in the response. Therefore, positive LuxR autoregulation is required for a bistable response in the framework of our model.

Validating model predictions: dependence of *lux01* output on glucose

In addition to positive autoregulation, bistability is predicted to be critically dependent on the existence of basal constitutive *luxR* expression, as bistability is lost when $c_0=0$ and thus $\delta=0$. The model also predicted that the range of $[AI_{ex}]$ spanning the region of bistability would expand with increasing ratio of the rates of inducible to constitutive *luxR* transcription, γ/δ. Owing to the fact that the rate of *luxR* transcription is regulated in part by occupancy of the cAMP–CRP-binding site, the range of $[AI_{ex}]$ in which LuxR bistability could occur was predicted to expand as the concentration of glucose decreased. This effect can be seen both in the bifurcation histogram in Figure 3A and in a more direct representation of bistability of R (=[LuxR]) expression as a function of $1/\sqrt{\beta}$, which in turn is proportional to A (=[AI]) (Figure 3B). The maximum *luxR* expression was predicted to rapidly diminish with increasing glucose and correspondingly decreasing [cAMP–CRP], whereas the bistability range was expected to shift to higher [AI] under the same conditions.

To test the model predictions, the *lux01* circuit response was analyzed at different glucose levels. Analysis of the response using the aforementioned dilution techniques in media with different glucose concentrations (0, 1.5 and 2.5 mM) confirmed the model predictions (Figure 3C). As discussed above, in RM minimal medium supplemented with succinate, hysteresis occurred in the range of 0–50 nM AI. In agreement with the model, smaller $[AI_{ex}]$ ranges yielding bistable responses were seen when glucose concentration was increased. Moreover, the bistability ranges progressively shifted to higher $[AI_{ex}]$ with increasing glucose and the maximal response decreased, as was also predicted by the model (Figure 3B). Hence, these experimental results support the model that is consistent with positive LuxR autoregulation leading to a hysteretic dependence on fixed $[AI_{ex}]$.

It would be informative to show more directly that LuxR-positive transcriptional autoregulation plays a key role during the hysteretic response, e.g. if *luxR* expression could be controlled by an inducible promoter other than its native

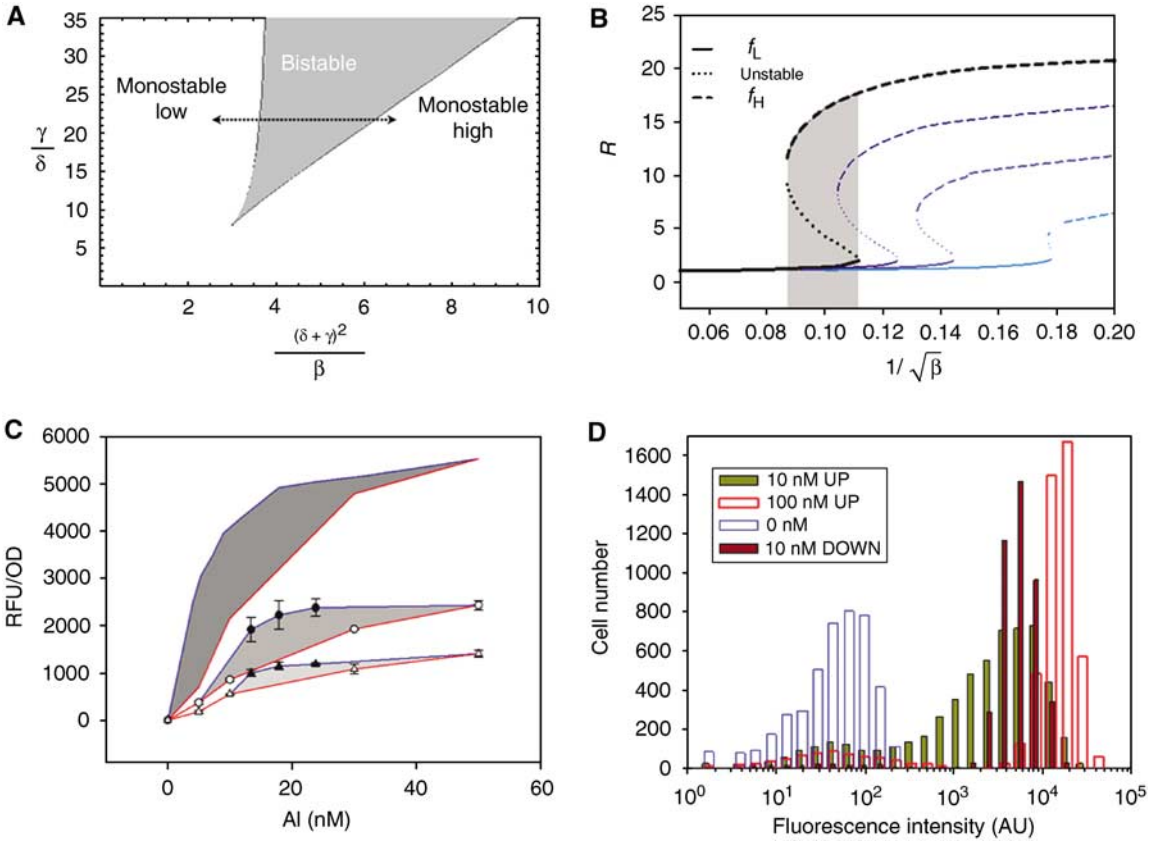

Figure 3 Mathematical modeling and experimental analysis of the *lux01* circuit response. (**A**) The model analysis predicts the existence of a domain of non-dimensional parameters characterizing the influence of AI and cAMP–CRP (see the text for the parameter description) on the number and stability of the steady states. The variation of [AI] is equivalent to moving on this graph parallel to the *X* axis. The bistability curve describing the expression of *luxR* as a function of [AI] corresponding to the dashed line with arrows is shown in black in (B). (**B**) The predicted dependencies of *luxR* expression (*R*) on [AI] (proportional to $1/\sqrt{\beta}$) for δ=1 and γ=20 (black), 16, 12, 8 (increasing lightness of the blue color). The bistability region corresponding to the overlap of two stable response branches f_L and f_H is shaded in gray. Note the progressive decrease in both the magnitude of responses and the location and the extent of the bistability regions. (**C**) Experimental analysis of the regions of hysteresis for glucose concentrations of 2.5 (light gray), 1.5 (medium gray) and 0 mM (dark gray, copied from Figure 1C for comparison). Red lines indicate induction from low [AI_{ex}] and blue lines indicate dilution from high [AI_{ex}]. Note the reduction of the bistability ranges and the decrease in the response amplitudes with increasing glucose, in agreement with the predictions in (B). Error bars represent the standard deviation of two independent triplicate sets. (**D**) Flow cytometry analysis of the hysteresis in *lux01* single cell response. The results are given as histograms corresponding to different modes of response induction: 'UP' for the induction for 7 h from the initial [AI_{ex}]=0 nM to [AI_{ex}]=10 nM, and 'DOWN' for the dilution experiment from the initial [AI_{ex}]=100 nM to [AI_{ex}]=10 nM. The histograms of the 'UP' induction experiments for the final [AI]=100 nM and the uninduced control (0 nM) are shown for comparison.

promoter. However, when this was attempted, it was found to be extremely difficult to maintain the levels of LuxR production in a physiologically relevant range. Specifically, a *luxR* deletion was generated in the *lux*01 circuit construct and *luxR* was expressed from a plasmid under the control of P_{tac} or P_{gcvR}. LuxR production from a pEXT22-based vector (1–1.5 copies per cell; Dykxhoorn *et al*, 1996) with the P_{tac} promoter was so high that it nearly saturated the response with as little as 1 nM AI (data not shown). A pPROBE′GFP tagless (Miller *et al*, 2000) construct with a low-level constitutive promoter P_{gcvR} from the *E. coli gcvR* gene (Ghrist and Stauffer, 1998) yielded GFP levels at less than 10% the normal maximum steady-state response even in the presence of 500 nM AI (data not shown). These findings further illustrate the importance of LuxR levels to the precise control of the QS response. Although using glucose levels in the medium to manipulate LuxR levels does not eliminate LuxR-positive feedback, it does allow for an analysis of the effect of different expression levels of LuxR, in a physiologically relevant manner. The observation that decreasing the levels of LuxR production in this manner also leads to a decrease in the degree of hysteresis implies that elimination of LuxR-mediated positive feedback would completely eliminate this behavior from the system. Indeed, a recent analysis of different synthetic LuxR–LuxI-based genetic circuits strongly suggested the absence of hysteresis in the response of a plasmid-based circuit analogous to the *lux01* circuit, when investigated in glucose-rich medium (Haseltine and Arnold, 2008).

Response bistability on a single-cell level

Population-level measurements can hide the details of the distribution of single-cell responses. To investigate the *lux01* response on the single-cell level, cell samples from the induction and 25% hourly dilution experiments were analyzed using flow cytometry (Figure 3D; Supplementary Figures S2–S5). For all [AI_{ex}] values, the cellular populations were well described by bimodal distributions. The lower fluorescence

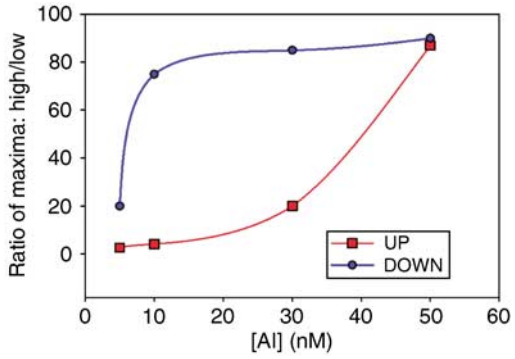

Figure 4 Comparison of the response peak maxima obtained from flow cytometry analysis of the *lux01* circuit induced to, and diluted from 100 nM AI_{ex}. The amplitude ratios of coinciding fluorescence peak values obtained from flow cytometry analysis of the *lux01* circuit induced from 0 to 100 nM AI_{ex} (UP), and diluted from a high state of induction obtained after 7 h induction at 100 nM AI_{ex} (DOWN) are shown for several concentrations of AI_{ex}. The data are represented as the ratio of fluorescence values of the maxima of the high/low peaks for UP and DOWN experiments as a function of $[AI_{ex}]$. Data are representative of two independent triplicate sets.

peaks for $[AI_{ex}]$=5 and 10 nM had peak fluorescence intensities virtually indistinguishable from that of the unimodal distribution of the uninduced cell population ($[AI_{ex}]$=0). As $[AI_{ex}]$ increased to 100 nM, both peaks of the bimodal distributions gradually shifted to higher fluorescence intensity values, with the maximum increase of the lower peak being about three-fold versus uninduced control. The peak fluorescence intensity of the higher response sub-population, which at $[AI_{ex}]$=10 nM was approximately 70-fold higher than the peak fluorescence of the lower response sub-population, also shifted with $[AI_{ex}]$. As a result, at $[AI_{ex}]$=50 or 100 nM, the position of the higher peak exceeded that of the lower peak by almost two orders of magnitude. As $[AI_{ex}]$ increased, the relative amplitude of the second peak also progressively increased, and that of the first peak decreased. There was no noticeable difference between the distributions corresponding to 7 and 14 h of induction, further suggesting that at 7 h post-induction the response is close to being maximally induced (data not shown).

When AI was diluted from the media of the cells in a highly induced state (7 h in $[AI_{ex}]$=100 nM) and assayed at various final $[AI_{ex}]$, the response distributions were also bimodal. However, although the positions of the response peaks coincided with those found in the induction experiment (induction of the response from low initial $[AI_{ex}]$), the relative amplitudes of the peaks were distinct, with the amplitude of the lower response peak considerably diminished. By plotting the ratio of the high to low maxima as a function of $[AI_{ex}]$, a hysteretic bistable response is clearly demonstrated for these coinciding peaks (Figure 4). There is approximately an 80-fold difference between the two steady states of expression that the response can achieve within the 0–50 nM range of $[AI_{ex}]$. These results suggested that each point used to obtain different null clines in Figure 1C was an average of two modes of response, and the hysteresis was a consequence of different weights placed on these modes by the history of the response induction. The results are consistent with the notion that response bimodality is a reflection of underlying response bistability coupled with the effects of molecular noise over prolonged periods of time, as recently shown in other well-characterized signaling and genetic systems (Gardner *et al*, 2000; Ozbudak *et al*, 2004; Paliwal *et al*, 2007). Bistability is commonly a reflection of underlying positive feedback, further implying that hysteresis and bimodality in the response of the *lux*01 circuit depends on the presence of a second, LuxI-independent feedback loop in the system.

Noise reduction due to LuxR upregulation

Occupancy of LuxR by AI can be viewed for each individual LuxR molecule as a binary variable (i.e. either LuxR is occupied or not). Thus, occupancy of many LuxR molecules could be represented as a series of Bernoulli trials, with the average and standard deviation given by the binomial distribution. The probability that an individual receptor is occupied is given by:

$$P = \frac{A}{A + \tilde{K}_D} \tag{7}$$

where A=[AI] and $\tilde{K}_D$ is the affinity of AI to LuxR. Correspondingly, the probability that a LuxR molecule is not occupied by AI is:

$$q = \frac{\tilde{K}_D}{A + \tilde{K}_D} \tag{8}$$

Therefore, for the binomial distribution of occupancy levels, we have the mean:

$$\mu = np = \frac{nA}{A + \tilde{K}_D} \tag{9}$$

where n is the number of LuxR molecules. For the ratio of the standard deviation to the mean (the coefficient of variation), a frequently used metric of molecular noise, we have:

$$\eta = \frac{\sigma}{\mu} = \frac{\sqrt{np(1-p)}}{np} = \sqrt{\frac{1-p}{np}} = \sqrt{\frac{\tilde{K}_D}{nA}} \tag{10}$$

Thus, the molecular noise characterizing LuxR–AI-binding events scales as the inverse of the square root of the total number of LuxR molecules, making the response more robust if [LuxR] is upregulated. To evaluate η using the flow cytometry experiments (Figure 3D; Supplementary Figures S3–S5), we fitted the curves with a sum of two Gaussian distributions, corresponding to the constituent distributions, and estimated their mean and standard deviation values. The analysis suggested that the molecular noise, η, in the expression of *luxI* can decrease from 0.93 to 0.29 for [AI]=5 nM, and from 0.47 to 0.19 for [AI]=10 nM, confirming that an increase in the expression of *luxR* can indeed decrease the molecular noise in the QS response.

Examination of the *luxR/I* circuit

As explained above, the steady-state responses of the full *lux* operon can be obtained by considering the intersections of the null clines f and g^{-1}. Alternatively, the intersections of the related null clines: $[\mathrm{LuxR}] = [R] = \tilde{f}([\mathrm{AI}])$ and $[\mathrm{AI}] = \tilde{g}([\mathrm{LuxR}]) \propto 1/\sqrt{\beta}$, describing mutual dependencies between *luxR* expression and [AI] can be considered. The

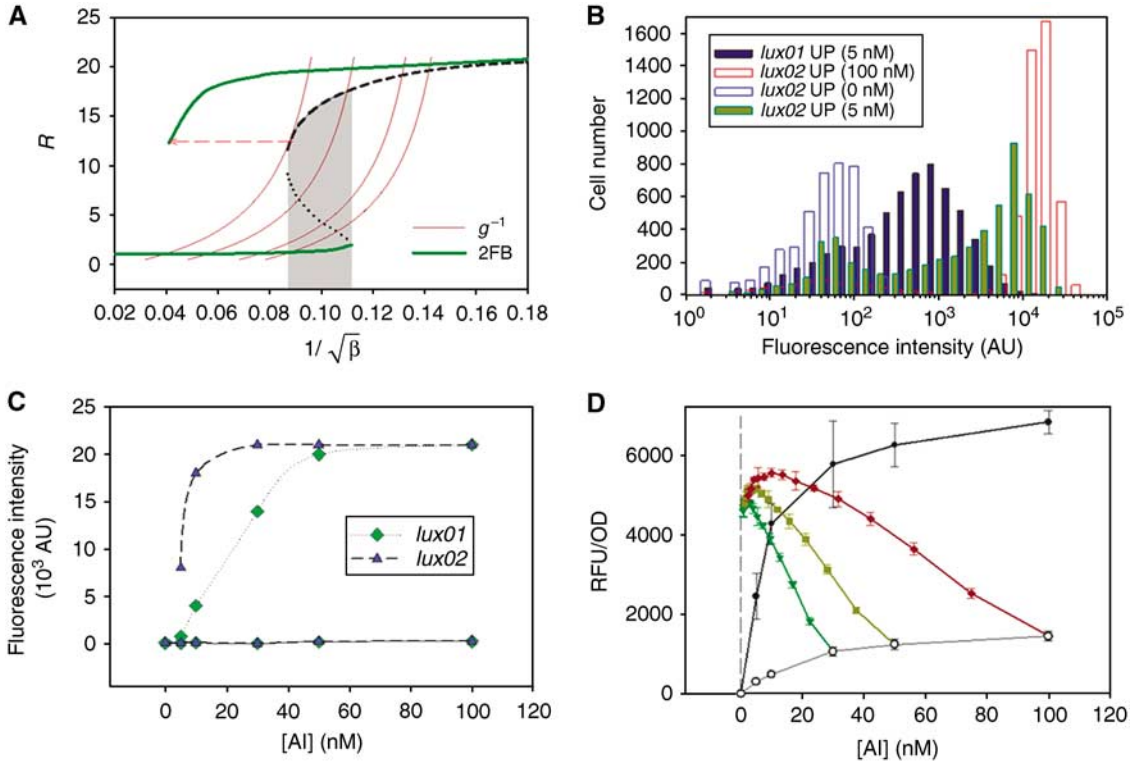

Figure 5 Mathematical modeling and experimental analysis of the *lux02* circuit response. (**A**) Graphical analysis of bistability in the presence of AI synthesis in the *lux02* circuit in the form of intersection of the bistable curve, $\tilde{f}([\mathrm{AI}])$ from Figure 2B (black) and the assumed series of curves representing the dependence of [AI] on the expression of *luxR* (as a proxy for *luxI* expression). These $\tilde{g}^{-1}([\mathrm{AI}])$ null clines are assumed to be of the form $\tilde{g}^{-1}([\mathrm{AI}]) = (G[\mathrm{AI}]/K + [\mathrm{AI}]) + [\mathrm{AI}_{\mathrm{ex}}]$, where K=5; $[\mathrm{AI}_{\mathrm{ex}}]$=0.02, 0.04, 0.06 and 0.07, and G=0.09. The curves resulting from the intersection of $\tilde{f}([\mathrm{AI}])$ and $\tilde{g}^{-1}([\mathrm{AI}])$ as a function of $[\mathrm{AI}_{\mathrm{ex}}]$ are shown in green, and the extension of the bistability range is indicated by the red arrow. (**B**) Flow cytometry analysis of the single cell responses of the *lux02* circuit exposed to $[\mathrm{AI}_{\mathrm{ex}}]$=5 nM contrasted with the responses of this circuit to $[\mathrm{AI}_{\mathrm{ex}}]$=0 and 100 nM, and with the response of the *lux01* circuit to $[\mathrm{AI}_{\mathrm{ex}}]$=5 nM. (**C**) The peak values of the fluorescence intensity distributions obtained from two cell response sub-populations of the *lux01* and *lux02* exposed to different $[\mathrm{AI}_{\mathrm{ex}}]$ values, obtained using flow cytometry experiments. (**D**) The 2 h (open circles) and 8 h (closed circles) induction curves are overlaid with 25% hourly AI dilution from the medium of cells expressing *lux02* from 30 (inverted triangles), 50 (squares) or 100 nM (diamonds) $[\mathrm{AI}_{\mathrm{ex}}]$, with the output converging to a constant level in spite of multiple rounds of cell and AI dilution from the medium. Error bars represent the standard deviation of two independent triplicate assays.

simulated null cline $\tilde{f}$, plotted in Figure 3B and reproduced in Figure 5A, describes bistability of the *lux01* circuit. Unfortunately, determination of the other null cline, $\tilde{g}$, is less straightforward for several reasons. First, although it is clear from our (data not shown) and other analyses that *luxR* overexpression positively regulates *luxI* expression, the details of *luxI* expression and AI synthesis as a function of LuxR autoregulation are poorly known. Second, as AI can diffuse into the space surrounding the cells, the effect of *luxR* expression on [AI] experienced by cells can depend on cell density, the rate of removal of AI from extracellular spaces, the geometry of extracellular spaces, and so on. We therefore simplified the analysis to assume that the [AI] experienced by cells depends on *luxR* expression as follows:

$$[\mathrm{AI}] = \frac{\sigma[\mathrm{LuxR}]}{[\mathrm{LuxR}] + \mathrm{K_{QS}}} + [\mathrm{AI_{Ex}}]$$

Thus, [AI] is assumed to have a saturable dependence on the expression of *luxR* (reaching the maximal value σ for very high LuxR levels), with the sensitivity to LuxR defined by the constant K_{QS}. In addition, [AI] can also be augmented by the addition of exogenous AI experimentally. This equation describes a series of null clines $\tilde{g}$, discussed above, which can be used to obtain the steady-state solutions for the whole QS circuit. Note that one reduces the problem to the case of the *lux01* circuit by putting σ=0, which would correspond to the null clines being perpendicular to the [AI] axis. This was implicitly done in our earlier analysis of Figure 3B. Any $\sigma \neq 0$ implies therefore that the corresponding null clines would intersect the higher stable branch of $\tilde{f}$ at values of $[\mathrm{AI}_{\mathrm{ex}}]$ higher than those of the *lux01* case, due to sloping of the $\tilde{g}$ null clines (see Figure 5A). In addition, as shown in Figure 5A, null clines for a larger range of $[\mathrm{AI}_{\mathrm{ex}}]$ can intersect with both stable branches of $\tilde{f}$, thus extending the hysteresis range. Therefore, generally speaking, if AI can be produced endogenously by the cells, one would expect increased values of LuxR for the higher steady-state response versus the *lux01* circuit case, for the same $[\mathrm{AI}_{\mathrm{ex}}]$. The hysteresis range would also be expected to increase.

To validate these predictions, we investigated the *lux02* circuit, which differs from the *lux01* circuit by having the capacity to express *luxI* and thereby synthesize AI (Supplementary Figure S1). Cells carrying the *lux02* circuit were grown in the presence of different [AI] in the range of 0–100 nM, to compare the response to that of the *lux*01 circuit. The response increased over the first 6 h, stabilizing at 7–8 h

(Supplementary Figure S6). Consistent with model predictions, the single cell response displayed bistability, with the higher steady-state distributions substantially exceeding (for $[AI_{ex}]$=0–10 nM) or closely coinciding (for $[AI_{ex}]$=10–100 nM) with those of the highest steady-state response distributions (for $[AI_{ex}]$=50 and 100 nM) of the *lux01* single cell responses. These results suggested that the coexistence of two coupled feedback loops can increase the degree to which the response can be induced at lower $[AI_{ex}]$.

The predicted expansion of the hysteresis range implied that the higher response steady state can exist at very low $[AI_{ex}]$, possibly even zero. One strategy to test this involved inducing the cell response by the addition of AI at specific values, followed by continuous cell and AI dilution. This insured dilution of exogenously added AI to values close to zero, which may or may not be compensated by AI secretion and cell induction to the higher response steady state. When 25% hourly dilutions of AI were performed with *lux02* circuit-expressing cells that had been weakly induced (2 h induction) at different initial $[AI_{ex}]$, not only did the population achieve its higher state of induction, it remained in that state throughout the experiment in spite of continuous removal of AI and cells (Figure 5D). The 25% per hour dilution rate appeared to match cell division and AI production rates by *lux02*-carrying cells, as at higher dilution rates, both the response was lost and cells were diluted out (data not shown). Overall, these results suggested that in a situation modeling the QS response in the context of a biofilm or a light organ, when the number of cells is relatively constant, the QS response can be induced and stably maintained even in the face of constant removal of AI.

Discussion

Using a combination of mathematical modeling and experimental analysis, we have shown that the regulation of expression of *luxI* during the *V. fischeri* QS response exhibits complex hysteretic dependency on the $[AI_{ex}]$, due to AI-dependent autoregulation of *luxR* expression. In particular, *luxI* expression can assume two distinct levels in response to fixed $[AI_{ex}]$ within the 0–50 nM range. The chosen response value depends on whether there is a recent history of cell exposure to high [AI]. Thus, in the full *lux operon*, two nested feedback loops can control the onset and maintenance of the collective cell responses. This combination of feedback responses adds to a growing list of the functionally important nested feedback systems, including multiple feedbacks regulating galactose utilization in yeast (Acar *et al*, 2005) and a combination of positive and negative feedback loops in many other natural and synthetic circuits (Tsai *et al*, 2008).

A number of important advantages can be gained from this type of feedback loop architecture. One important consideration for this circuit is that LuxI-mediated feedback is distinct from a classical cell-autonomous type of feedback in that AI does not remain within or around a single cell, but rather it is shared among the cells within a population, thus coupling their responses. Therefore, the extent to which this feedback occurs depends on the local cell microenvironment, including cell density, geometric constraints and the rate of AI removal (Hense *et al*, 2007). This uncertainty in the feedback circuit regulation has the potential of making the circuit performance less robust and more subject to perturbations in the environment. Hence an additional level of response control, provided by *luxR* transcriptional autoregulation, can facilitate establishment of a cell sub-population, that once induced, continues to stably display QS, even if the local [AI] undergoes transient or persistent reduction. The memory of QS induction is maintained in the population due to a high level of LuxR, and thus a relatively high level of LuxR–AI complexes, even if [AI] is decreased.

A complimentary advantage is response diversification. Although response diversification can arise in many bistable systems with substantial amounts of molecular noise, the range of concentrations under which bistability can occur can be substantially augmented in the presence of two coupled feedback loops (Figure 5). This further implies that, under a wide range of extracellular conditions, two sub-populations may emerge, the responses of which can exist at two distinct stable states. The higher stable response state, in which most cells would predominantly reside, would mediate the QS response. At the same time, the less abundant lower response state would represent a reservoir of cells that can quickly displace the higher response state cells, due to a decreased metabolic load associated with lower levels of *luxR* and *luxI* expression. Should the conditions dramatically change (e.g. due to removal of most of the population), a fast replenishment of the uninduced population would ensue in a manner not dependent on the gradual decrease of LuxR and LuxI levels by degradation and cell growth-related dilution. This small cell reservoir, capable of replenishing the population following a major alteration of the surrounding medium, is not unlike the reservoir of persister cells resistant to the level of antibiotics capable of killing most of a population in a situation such as a biofilm (Balaban *et al*, 2004). Thus, the QS circuit appears to combine two distinct strategies previously proposed for how a cell population can best respond to a changing environment (Kussell and Leibler, 2005). It can both adapt to an increased cell population by progressive upregulation of the QS response, and diversify the response as a means of coping with catastrophic changes in cell numbers and [AI].

The concentration of glucose is also a key parameter to consider, as cAMP–CRP levels control the levels of *luxR* transcriptional regulation, which determines whether or not full QS induction can be achieved and robustly maintained over a wide range of $[AI_{ex}]$. Interestingly, Friedrich and Greenberg (1983) also saw evidence that *V. fischeri* cells grown in chemostats had a memory of their previous exposure to glucose during QS. Importantly, the corresponding dependence of luminescence on active CRP may facilitate the establishment and maintenance of the symbiosis between *V. fischeri* and its squid host. The host may be capable of controlling the onset of QS by providing lower levels of glucose at a lower cell density, which would trigger induction earlier than a dense population under higher initial nutrient levels. This bacterial–host interaction thus represents yet another potential feedback system, stabilizing the level of luminescence output.

In addition to cAMP–CRP regulation of *luxR*, LuxR autoregulation affords a mechanism to increase the precision of AI sensing by the cells. Indeed, cells can mount a significant

response to [AI] as low as 5 nM. This concentration, for the typical *E. coli* and *V. fischeri* cell volumes of a few femptoliters, translates into less than 10 molecules of AI per cell. This is a very small number, likely subject to significant variation, or molecular noise within a cell, which could lead to pronounced noise in signaling output. This study has shown both analytically and experimentally, that upregulation of *luxR* expression could considerably reduce this noise, with as much as a three-fold reduction in the variability of LuxR–AI binding and ensuing transcriptional regulation for $[AI_{ex}]=5$ nM.

Upregulation of LuxR can also serve to control regulation of other genes in the *lux* regulon. At least three other members of the *lux* regulon, *qsrP*, *acf* and *ribB* have lower affinities for LuxR–AI complexes compared with that of the *luxI* promoter (Qin *et al*, 2007). Upregulation of *luxR* expression may increase the expression of these genes following the onset of QS, while maintaining them at a low level during the initial stages of the response.

In the native host, *V. fischeri*, additional upstream signal-transduction pathways and regulators might also have an influence on *luxR* expression rates. However, utilizing a simplified genetic circuit in recombinant *E. coli* has enabled an analysis of how the available pools of LuxR and AI ultimately modulate the response. Development of a quantitative understanding of this isolated genetic circuit can both help elucidate the more complex behavior of the native QS response, and assist in synthetic biology efforts where such interspecies transfer of parts of genetic networks, including the *lux* operon, is very common (i.e. Buchler *et al*, 2003).

In conclusion, these results provide a comprehensive picture of the ability of the basic LuxR/I genetic system, which is a common motif of many QS circuits, to favor and maintain a high level of expression of its target genes once a certain threshold of expression is reached. It would seem logical that the hindrance of this activation would be the most effective way to prevent high-level expression of QS-controlled genes, because shutting down an activated system would be difficult in natural settings, such as during tissue infections, symbiosis, or biofilm formation.

Materials and methods

Strains and growth conditions

To create *E. coli* MG1655-01S (*lux*01 circuit; *luxR* divergently transcribed from P_{luxI} fused to *gfp*) and MG1655-02S (*lux*02 circuit; *luxR* divergently transcribed from *luxI* fused to *gfp*) (Supplementary Figure S1), *lux* operon fragments were removed through *Eco*RI–*Kpn*I, and *Eco*RI–*Bam*HI restriction digestions from pLVA01 and pLVA02, respectively (Groisman *et al*, 2005) and placed into the multiple cloning site (MCS) of pPROBE′-GFP-Tagless which encodes a stable GFP (Miller *et al*, 2000) as a transcriptional reporter. These reporter fragments were then removed through *Eco*RI–*Not*I digestion and ligated into the λInCh vector, a modified pDHB60 (Boyd *et al*, 2000). The pDHB60 vector had been modified by the (1) removal of the P_{tac} promoter through *Eco*RI–*Bam*HI digestion, (2) ligation with an *Eco*RI–*Bam*HI fragment of pPROBE′-GFP (LAA) containing its MCS and (3) adding a *Not*I site between the *Eco*RI and *Xba*I sites. This modified pDHB60 was ligated with the *lux-gfp* reporter cassettes and used in the λInCh insertion protocol to place the expression cassettes into the *E. coli* MG1655 chromosome, generating stable, single-copy expression systems (Boyd *et al*, 2000). During cloning stages, strains were grown, shaking at 250 r.p.m. and 37°C in Luria–Bertani broth (containing 100 μg/ml ampicillin (Ap) and 50 μg/ml kanamycin (Kn), as necessary). During the analyses for hysteresis, strains were grown, shaking at 250 r.p.m. in RM minimal medium (2% casamino acids, 1 × M9 salts (12.8 g Na_2HPO_4 $7H_2O$, 3 g KH_2PO_4, 0.5 g NaCl and 1 g NH_4Cl per liter), 1 mM $MgCl_2$) with 0.4% succinate and 25 μg/ml Ap at 30°C, unless otherwise indicated.

Gradual hourly dilution of AI from induced cultures

E. coli MG1655-01S or -02S were grown overnight at 37°C in RM minimal medium with succinate and 25 μg/ml Ap. The overnight culture was subcultured into the same medium to an OD_{590} of 0.15. Prior to subculturing, samples were centrifuged, the supernatant was discarded and the pellet was resuspended in a fresh medium twice to eliminate any AI carry over. The culture was incubated at 30°C with shaking until an OD_{590} of 0.25 was reached. At this point, 5 ml aliquots of culture were added to tubes that contained known amounts of dried AI. These induced cultures were incubated for various times, up to 7 h (depending on the type of analysis) at 30°C with shaking.

Here, 25% dilutions were performed by adding 3.75 ml of the induced culture to 1.25 ml of pre-warmed fresh RM minimal medium without AI. Prior to dilution, 200 μl of culture was placed in a 96-well optical bottom microtiter plate for the analysis of both fluorescence output (excitation and emission wavelengths of 485 and 535 nm, respectively) and OD_{590} on a Tecan SpectraFluor Plus plate-reader (Tecan, Mannedorf/Zurich, Switzerland). Fluorescence values were corrected for background by subtracting the RFU obtained from an uninduced culture of MG1655-01S at comparable cell density, and the per cell output was determined by dividing the corrected RFU by the OD. The procedure was repeated hourly to achieve a gradual dilution of the AI in the medium and maintain the culture in the mid-exponential phase of growth. Assays were performed as two independent triplicate sets. A major concern for the analysis of hysteresis was that any differences observed between diluted cultures and undiluted controls, allowed to grow to high steady-state expression, could be caused by changes in cell physiology due to the controls reaching stationary phase. To ensure that this did not occur, control cultures were not allowed to reach an OD_{590} higher than 1.0. The manner in which the dilution assays were performed maintained all of the diluted cultures between an OD_{590} of 0.4 and 0.7. Hence, the cells were maintained in the exponential phase over extended periods beyond that of normal batch culture.

Instantaneous serial dilution of AI from induced cultures

A more conventional method for testing hysteresis is to induce to a maximum steady state, and then dilute the AI from the system. To perform this type of assay, cultures were induced as described above, for 7 h prior to dilution, which corresponds to near maximum levels of QS induction for the system. Induced cultures were serially diluted 25% by combining and mixing two 5 ml induced cultures (induced at the same [AI]) and adding 9 ml of this culture to 3 ml of pre-warmed RM minimal medium; 9 ml of the first dilution was used to make the second dilution. This was repeated for a total of seven dilutions. At 1 and 2 h post-dilution, 200-μl samples were taken and analyzed as described above. Assays were performed as three independent trials.

Modulation of the QS response by glucose addition

E. coli MG1655-01S cultures grown in RM minimal medium with succinate were supplemented with glucose concentrations up to 10 mM. A 25% gradual hourly dilution of AI assay was performed as above, using dilution medium containing the same concentration of glucose as the original culture. If the induction period was longer than 2 h, 1 ml of culture was replaced with 1 ml of fresh medium containing the same concentration of glucose and AI every hour starting at hour 4. This ensured that the culture was maintained in mid-exponential phase until the dilution assay began at either 6 or 8 h induction, and

that the glucose in the medium did not become depleted. Culture density and fluorescence were measured as described above.

qRT–PCR analysis of luxR transcript levels

When undiluted cultures had been induced for 6 h, 500 µl was added to 1 ml of Qiagen RNAprotect Bacteria Reagent (Qiagen, Valencia, CA). Samples were stored at −70°C until the RNA was extracted according to the Qiagen RNA spin mini kit and stored at −70°C. RNA was analyzed for quality and concentration, converted to cDNA through the Applied Biosystems High-Capacity cDNA Reverse Transcription Kit protocol (Applied Biosystems, Foster City, CA) and stored at −20°C. The cDNA samples were then used as templates in an Applied Biosystems 7300 Real-Time PCR system. The primers used during the PCR reaction to amplify a region of *luxR* were 5′ TGGCAGCGGT TAGTTGTATTG 3′ and 5′ TAGCGTGGGCGAGTGAAG 3′. Here, 50 ng of cDNA was used as template, with primer concentrations at 250 nM. SYBR Green master mix (2 ×) (Applied Biosystems) and dH_2O were added to a final reaction volume of 50 µl per well in a MicroAmp Optical 96-well Reaction Plate (Applied Biosystems). The thermal cycler settings were programmed for 52°C for 2 min, 95°C for 10 min, then 45 cycles of the following: 95°C for 15 s, 52°C for 15 s and 60°C for 1 min, which was also set as the data collection point. Three independent samples were analyzed in triplicate.

Flow cytometry analysis

Cultures of *E. coli* MG1655-01S or *E. coli* MG1655-02S were grown and induced with AI as stated earlier. At 7 h induction, samples were diluted as per the 25% hourly dilution of AI protocol listed above. Here, 500-µl samples were taken at each hourly time point and pelleted through centrifugation at 14 000 r.p.m. for 2 min at 4°C. Cells were then resuspended in cold PBS (0.2 M potassium phosphate monobasic and 0.2 M sodium chloride, pH 7) containing 100 µg/ml chloramphenicol, and placed on ice overnight. The following day, samples were analyzed at the flow cytometry lab at the Virginia-Maryland Regional College of Veterinary Medicine on a BD (Becton Dickinson) FACS Aria flow cytometer. Data for two independent sets was collected using the software FlowJo version 7 (Tree Star). All cells producing a fluorescent signal were counted in the gating so that an accurate distribution of expression across the entire population would be achieved.

Supplementary information

Supplementary information is available at the *Molecular Systems Biology* website (www.nature.com/msb).

Acknowledgements

We thank Joan Kalnitsky and Melissa Makris for assistance in performing flow cytometry and Steven Lindow for providing the *gfp* transcriptional fusion vectors. This research was supported by NIH R01 GM066786, NSF IGERT DGE-0504196 and the Virginia Tech Graduate Research Development Program.

Conflict of interest

The authors declare that they have no conflict of interest.

References

Acar M, Becskei A, van Oudenaarden A (2005) Enhancement of cellular memory by reducing stochastic transitions. *Nature* **435:** 228–232

Angeli D, Ferrell Jr JE., Sontag ED (2004) Detection of multistability, bifurcations, and hysteresis in a large class of biological positive-feedback systems. *Proc Natl Acad Sci USA* **101:** 1822–1827

Balaban NQ, Merrin J, Chait R, Kowalik L, Leibler S (2004) Bacterial persistence as a phenotypic switch. *Science* **305:** 1622–1625

Boyd D, Weiss SD, Chen JC, Beckwith J (2000) Towards single copy gene expression systems making gene cloning physiologically relevant: lambda InCh, a simple *Escherichia coli* plasmid-chromosome shuttle system. *J. Bacteriol* **182:** 842–847

Buchler NE, Gerland U, Hwa T (2003) On schemes of combinatorial transcription logic. *Proc Natl Acad Sci USA* **100:** 5136–5141

Chatterjee J, Miyamoto CM, Meighen EA (1996) Autoregulation of *luxR*: the *Vibrio harveyi lux*-operon activator functions as a repressor. *Mol Microbiol* **20:** 415–425

Choi SH, Greenberg EP (1992) Genetic dissection of DNA binding and luminescence gene activation by the *Vibrio fischeri* LuxR protein. *J Bacteriol* **174:** 4064–4069

Cox CD, Peterson GD, Allen MS, Lancaster JM, McCollum JM, Austin D, Yan L, Sayler GS, Simpson ML (2003) Analysis of noise in quorum sensing. *Omics* **7:** 317–334

Dunlap PV, Greenberg EP (1985) Control of *Vibrio fischeri* luminescence gene expression in *Escherichia coli* by cyclic AMP and cyclic AMP receptor protein. *J Bacteriol* **164:** 45–50

Dunlap PV, Greenberg EP (1988) Control of *Vibrio fischeri lux* gene transcription by a cyclic AMP receptor protein–LuxR protein regulatory circuit. *J Bacteriol* **170:** 4040–4046

Dunlap PV, Ray JM (1989) Requirement for autoinducer in transcriptional negative autoregulation of the *Vibrio fischeri luxR* gene in *Escherichia coli*. *J Bacteriol* **171:** 3549–3552

Dykxhoorn DM, St Pierre R, Linn T (1996) A set of compatible *tac* promoter expression vectors. *Gene* **177:** 133–136

Ferrell Jr JE (2002) Self-perpetuating states in signal transduction: positive feedback, double-negative feedback and bistability. *Curr Opin Cell Biol* **14:** 140–148

Friedrich WF, Greenberg EP (1983) Glucose repression of luminescence and luciferase in *Vibrio fischeri*. *Arch Microbiol* **134:** 87–91

Fuqua C, Parsek MR, Greenberg EP (2001) Regulation of gene expression by cell-to-cell communication: acyl-homoserine lactone quorum sensing. *Annu Rev Genet* **35:** 439–468

Gardner TS, Cantor CR, Collins JJ (2000) Construction of a genetic toggle switch in *Escherichia coli*. *Nature* **403:** 339–342

Ghrist AC, Stauffer GV (1998) Promoter characterization and constitutive expression of the *Escherichia coli gcvR* gene. *J Bacteriol* **180:** 1803–1807

Goryachev AB, Toh DJ, Lee T (2006) Systems analysis of a quorum sensing network: design constraints imposed by the functional requirements, network topology and kinetic constants. *Biosystems* **83:** 178–187

Groisman A, Lobo C, Cho H, Campbell JK, Dufour YS, Stevens AM, Levchenko A (2005) A microfluidic chemostat for experiments with bacterial and yeast cells. *Nat Methods* **2:** 685–689

Haseltine EL, Arnold FH (2008) Implications of rewiring bacterial quorum sensing. *Appl Environ Microbiol* **74:** 437–445

Hense BA, Kuttler C, Muller J, Rothballer M, Hartmann A, Kreft JU (2007) Does efficiency sensing unify diffusion and quorum sensing? *Nat Rev Microbiol* **5:** 230–239

James S, Nilsson P, James G, Kjelleberg S, Fagerstrom T (2000) Luminescence control in the marine bacterium *Vibrio fischeri*: an analysis of the dynamics of *lux* regulation. *J Mol Biol* **296:** 1127–1137

Kaplan HB, Greenberg EP (1985) Diffusion of autoinducer is involved in regulation of the *Vibrio fischeri* luminescence system. *J Bacteriol* **163:** 1210–1214

Kussell E, Leibler S (2005) Phenotypic diversity, population growth, and information in fluctuating environments. *Science* **309:** 2075–2078

Levchenko A (2003) Dynamical and integrative cell signaling: challenges for the new biology. *Biotechnol Bioeng* **84:** 773–782

Lupp C, Urbanowski M, Greenberg EP, Ruby EG (2003) The *Vibrio fischeri* quorum-sensing systems *ain* and *lux* sequentially induce luminescence gene expression and are important for persistence in the squid host. *Mol Microbiol* **50:** 319–331

Miller WG, Leveau JHJ, Lindow SE (2000) Improved *gfp* and *inaZ* broad-host-range promoter-probe vectors. *Mol Plant Microbe Interact* **13:** 1243–1250

Minogue TD, Wehland-von Trebra M, Bernhard F, von Bodman SB (2002) The autoregulatory role of EsaR, a quorum-sensing regulator in *Pantoea stewartii* ssp. *stewartii*: evidence for a repressor function. *Mol Microbiol* **44:** 1625–1635

Muller J, Kuttler C, Hense BA, Rothballer M, Hartmann A (2006) Cell–cell communication by quorum sensing and dimension-reduction. *J Math Biol* **53:** 672–702

Ninfa AJ, Mayo AE (2004) Hysteresis vs. graded responses: the connections make all the difference. *Sci STKE* **2004:** 20

Ozbudak EM, Thattai M, Lim HN, Shraiman BI, von Oudenaarden AV (2004) Multistability in the lactose utilization network of *Escherichia coli*. *Nature* **427:** 737–740

Paliwal S, Iglesias PA, Campbell K, Hilioti Z, Groisman A, Levchenko A (2007) MAPK-mediated bimodal gene expression and adaptive gradient sensing in yeast. *Nature* **446:** 46–51

Qin N, Callahan SM, Dunlap PV, Stevens AM (2007) Analysis of LuxR regulon gene expression during quorum sensing in *Vibrio fischeri*. *J Bacteriol* **189:** 4127–4134

Reading NC, Sperandio V (2006) Quorum sensing: the many languages of bacteria. *FEMS Microbiol Lett* **254:** 1–11

Sha W, Moore J, Chen K, Lassaletta AD, Yi C, Tyson JJ, Sible JC (2003) Hysteresis drives cell-cycle transitions in *Xenopus laevis* egg extracts. *Proc Natl Acad Sci USA* **100:** 975–980

Shadel GS, Baldwin TO (1991) The *Vibrio fischeri* LuxR protein is capable of bidirectional stimulation of transcription and both positive and negative regulation of the *luxR* gene. *J Bacteriol* **173:** 568–574

Shadel GS, Baldwin TO (1992) Positive autoregulation of the *Vibrio fischeri luxR* gene. LuxR and autoinducer activate cAMP–catabolite gene activator protein complex-independent and -dependent luxR transcription. *J Biol Chem* **267:** 7696–7702

Stevens AM, Greenberg EP (1999) *Transcriptional Activation by LuxR: Cell–Cell Signaling in Bacteria*. ASM Press: Washington, DC

Taga ME, Bassler BL (2003) Chemical communication among bacteria. *Proc Natl Acad Sci USA* **100:** 14549–14554

Tsai TY, Choi YS, Ma W, Pomerening JR, Tang C, Ferrell Jr JE (2008) Robust, tunable biological oscillations from interlinked positive and negative feedback loops. *Science* **321:** 126–129

Tyson JJ, Chen KC, Novak B (2003) Sniffers, buzzers, toggles and blinkers: dynamics of regulatory and signaling pathways in the cell. *Curr Opin Cell Biol* **15:** 221–231

Waters CM, Bassler BL (2005) Quorum sensing: cell-to-cell communication in bacteria. *Annu Rev Cell Dev Biol* **21:** 319–346

Withers H, Swift S, Williams P (2001) Quorum sensing as an integral component of gene regulatory networks in Gram-negative bacteria. *Curr Opin Microbiol* **4:** 186–193